Bioconjugate Chemistry

Article

pubs.acs.org/bc

Effects of Polydopamine Functionalization on Boron Nitride Nanotube Dispersion and Cytocompatibility

This paper was originally submitted for the "Biofunctional Biomaterials: The Third Generation of Medical Devices", published as the July 15, 2015, issue of Bioconjugate Chemistry (Vol. 26, No. 7).

Marc A. Fernandez-Yague,[†] Aitor Larrañaga,[†,‡] Olga Gladkovskaya,[†] Alanna Stanley,[§] Ghazal Tadayyon,[†] Yina Guo,[∥] Jose-Ramon Sarasua,[‡] Syed A. M. Tofail,[∥] Dimitrios I. Zeugolis,[†,⊥] Abhay Pandit,[†] and Manus J. Biggs*[,†]

[†]Centre For Research in Medical Devices (CURAM) and [⊥]Regenerative Modular & Developmental Engineering Laboratory (REMODEL), National University of Ireland Galway (NUIG), Galway, Ireland

[‡]Department of Mining-Metallurgy Engineering and Materials Science & POLYMAT, School of Engineering, University of the Basque Country (UPV/EHU), 480130 Bilbao, Spain

[§]Department of Anatomy, National University of Ireland Galway (NUIG), Galway, Ireland

[∥]Department of Physics and Energy, and Materials and Surface Science Institute (MSSI), University of Limerick, Limerick, Ireland

Supporting Information

ABSTRACT: Boron nitride nanotubes (BNNTs) have unique physical properties, of value in biomedical applications; however, their dispersion and functionalization represent a critical challenge in their successful employment as biomaterials. In the present study, we report a process for the efficient disentanglement of BNNTs via a dual surfactant/polydopamine (PD) process. High-resolution transmission electron microscopy (HR-TEM) indicated that individual BNNTs become coated with a uniform PD nanocoating, which significantly enhanced dispersion of BNNTs in aqueous solutions. Furthermore, the cytocompatibility of PD-coated BNNTs was assessed in vitro with cultured human osteoblasts (HOBs) at concentrations of 1, 10, and 30 μg/mL and over three time-points (24, 48, and 72 h). In this study it was demonstrated that PD-functionalized BNNTs become individually localized within the cytoplasm by endosomal escape and that concentrations of up to 30 μg/mL of PD-BNNTs were cytocompatible in HOBs cells following 72 h of exposure.

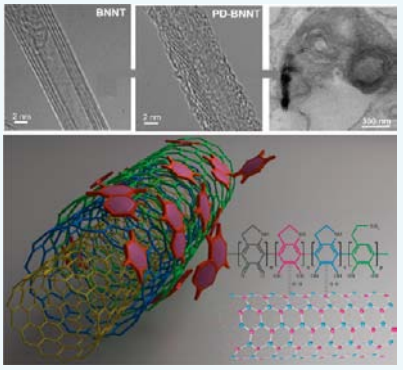

INTRODUCTION

The discovery of nanoscale carbon formulations encompassing one-dimensional nanotubes and two-dimensional graphene has resulted in significant advances in the fields of biomaterials and nanoelectronics. Boron nitride nanotubes (BNNTs), like carbon nanotubes (CNTs), have potential applications in both biomedical and nonconventional electronics thanks to their singular structural and physical properties.[1−4] Although CNTs have been largely studied as tubular nanostructures for a number of different applications,[5,6] BNNTs have only recently been explored as next generation materials.[7−9] BNNTs possess a similar physical structure to CNTs, yet possess significantly different physicochemical properties. In particular, despite the remarkable mechanical properties of CNTs, recent studies have demonstrated that BNNTs possess significantly greater shear strength than CNTs;[10] moreover, they have been shown to present higher thermal conductivity, superior electrical band gap properties, and are more resistant to oxidation at high temperatures.[11]

As with CNTs, in order to explore BNNTs as next generation materials it is crucial to develop cheap and facile methodologies for efficient dispersion and functionalization.[12] The difficulties associated with BNNT dispersion in water and organic solvents has proved problematic for the generation of BNNT formulations and nanocomposites, and early studies have concentrated on identifying suitable methodologies to address BNNT dispersion.[13−16] Initial approaches have focused on similar covalent and noncovalent methodologies used for CNT dispersion.[17] Specifically, acid treatment has been applied to add functional surface groups to CNTs; however, this treatment produces irreversible structural changes and decrements in electronic and mechanical properties of the nanotubes.[18−21] Alternatively, noncovalent approaches such as the use of amphiphilic molecules for dispersion have been successfully applied for CNT formulations[22−26] commonly in conjunction with an ultrasonication process.[27−33]

In the present work, functionalization of BNNTs with polydopamine chemistry (PD) was explored as a strategy to

Received: May 5, 2015
Revised: July 17, 2015
Published: August 17, 2015

DOI: 10.1021/acs.bioconjchem.5b00257
Bioconjugate Chem. 2015, 26, 2025−2037

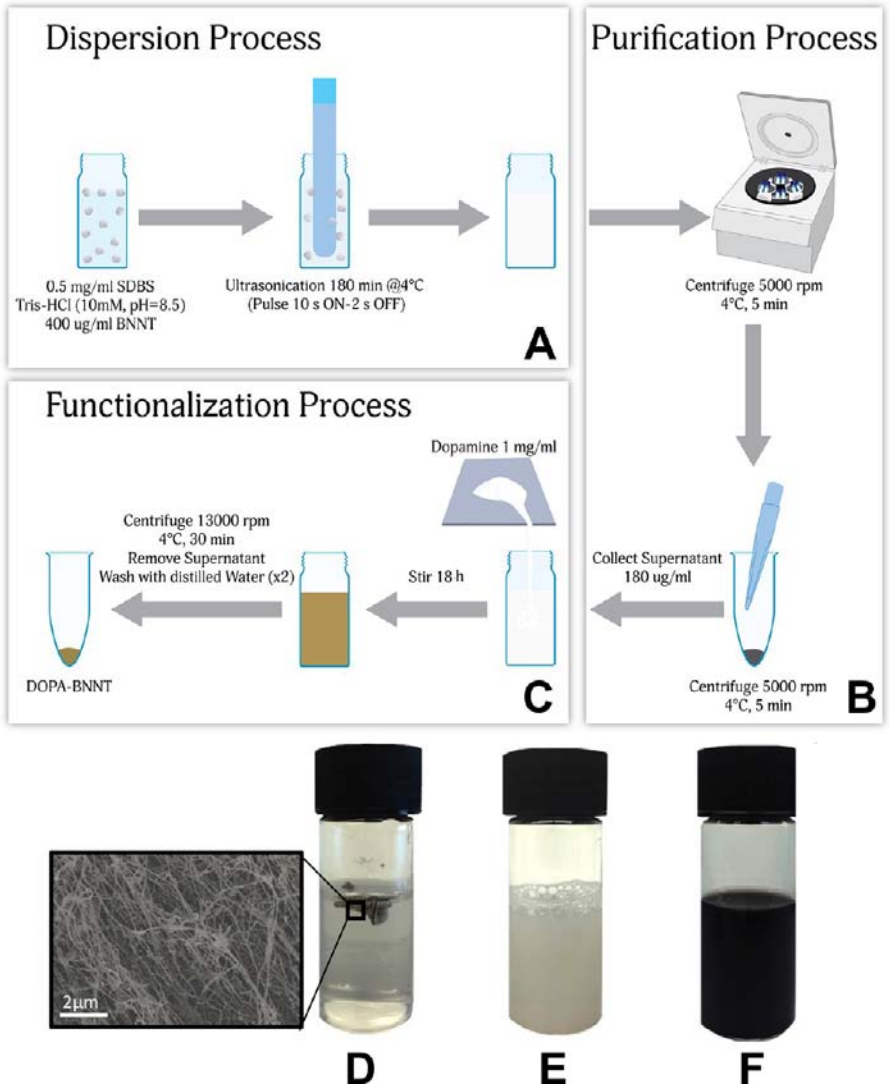

Figure 1. Schematic of the BNNT dispersion and PD-functionalization process. Pristine BNNTs were dispersed in Tris-HCL under probe ultrasonication to yield a 40 μg/mL suspension (A). BNNT suspension was subsequently centrifuged at 5000 rpm and the supernatant retained (B). The BNNTs were incubated with dopamine hydrochloride under agitation for 18 h before centrifugation at 13 000 rpm and washing (C). Pristine BNNTs retain a fibrous sponge-like morphology in aqueous environments following a 3 h sonication process (D). SDBS (0.5 mg/mL) facilitated dispersion of the BNNTs (E) which become functionalized with a stable PD nanocoating following the addition of dopamine hydrochloride (1 mg/mL) for 18 h (F).

improve the dispersion of BNNTs in aqueous solutions and to simultaneously provide functional groups that can act as anchorage points for further incorporation of molecules with biological activity, such as proteins or peptides.[34,35] PD is a dopamine derived synthetic eumelanin polymer that contains both catechol and amine functionalities in its backbone.[36,37] Via the simple immersion of a substrate in a dilute aqueous solution of dopamine hydrochloride, a thin PD layer can be deposited on the surface of a material. The aromatic molecules of dopamine strongly interact with boron nitride through $\pi-\pi$ stacking forces and van der Waals interactions. This approach has been explored as a strategy for dispersing many different micro- and nanoscale materials previously, including BNNTs and boron nitride platelets.[38,39] The results of these studies demonstrated improved dispersion in water and the generation of composite nanomaterials with enhanced mechanical and thermal properties.[40,41]

Interestingly, BNNTs possess a unique capacity to generate electric fields under mechanical stimulation (piezoelectricity),[12] and recent studies indicate that the piezoelectric response of BNNTs is higher than that of piezoelectric polymers such as PVDF.[42−45] In order to take advantage of these properties, BNNTs have been explored as nanovectors for intracellular release of drugs or for the delivery of electrical stimuli;[42] however, a greater understanding of BNNT cytocompatibility is critical to facilitate further investigation in this area.

The production of BNNTs by different methodologies such as CBD or ball-milling results in the synthesis of BNNTs with large diameters (30−50 nm) and nanotube formulations with a significant persistence of metallic impurities. Conversely, the BNNTs employed in this study were synthesized using a high-temperature pressurized vapor/condenser method (PVC). The BNNTs possessed between 1 and 5 discrete walls, a high aspect ratio (300 m^2/g), high crystallinity, and relatively small diameters (2−5 nm).

DOI: 10.1021/acs.bioconjchem.5b00257
Bioconjugate Chem. 2015, 26, 2025−2037

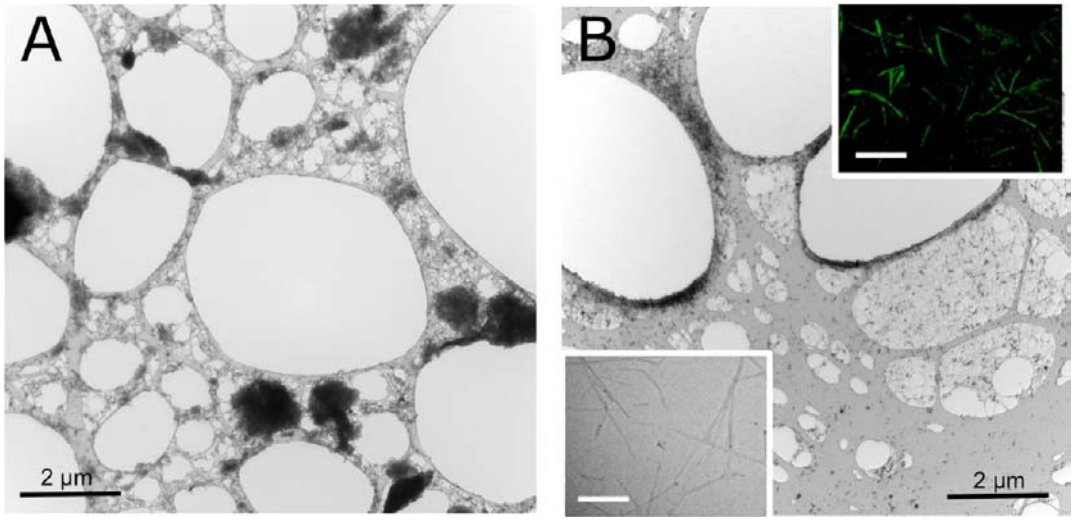

Figure 2. Low-magnification TEM images of non-functionalized and PD-functionalized BNNTs cast on lacey carbon grids. SDBS treated suspensions of BNNTS formed microaggregates in suspension (A). PD-functionalized BNNTs were observed to undergo a complete disentanglement, resulting in significantly enhanced dispersion (B). This was further confirmed via fluorescent imaging of peroxide activated autofluorescent BNNTs (insert). Inset scale bar, 1 μm.

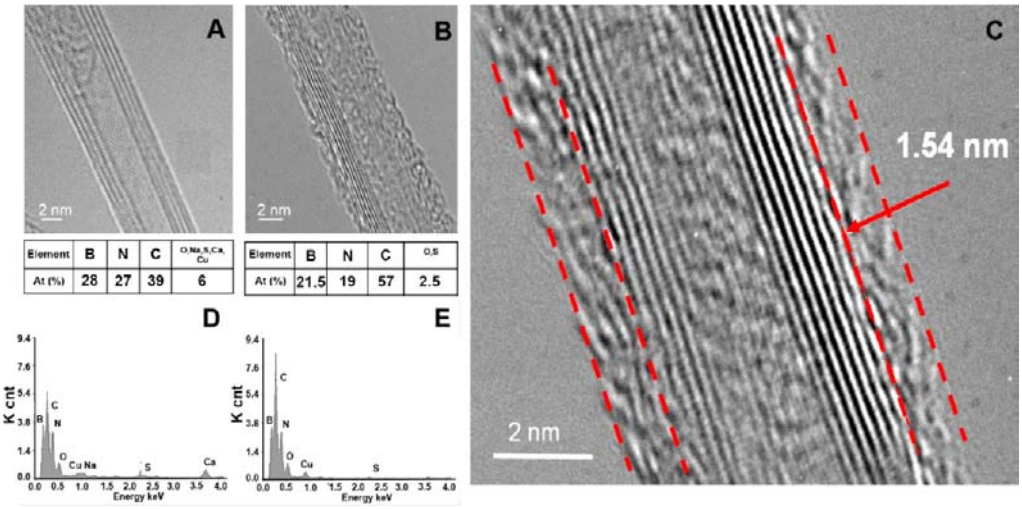

Figure 3. High-resolution TEM and EDS of SDBS dispersed and PD-functionalized BNNTs. SDBS dispersed BNNTs were observed to possess multiple well-defined walls and a hexagonal atomic arrangement. (A). Conversely, PD-functionalized BNNTs possessed an amorphous surface coating (B). Ultrahigh magnification (1.5 M) of this coating indicated the thickness of to be approximately 1.5 nm (C). Elemental analysis confirmed levels of boron, nitrogen, and sodium in SDBS dispersed BNNTs. (D) Conversely, boron, nitrogen, and sodium were reduced in PD-functionalized BNNTs and the presence of carbon increased (E).

Recent studies exploring BNNT cytocompatibility have concluded that the high hydrophobicity of the BNNTs resulting from the high polarity of the B−N bond leads to lower cytocompatibility than that of CNTs.[46] However, the degree of dispersion, incorporation of biocompatible coatings, and control over nanotube dimensions have yet to be explored as mediators of cytocompatibility. Considering BNNT cytocompatibility, PD is presented as a promising methodology to coat BNNTs for the generation of novel biomaterial formulations. Herein, we present the first study into the cytocompatibility of PD coated highly crystalline, small-diameter BNNTs produced by a catalyst-free, high-pressure, and high-temperature method.[11]

RESULTS

BNNT Dispersion in Tris-HCl Buffer. Figure 1A−1C shows representative images illustrating the process of BNNT PD coating and dispersion in a Tris-HCl solution. BNNTs were originally in the form of a dry sponge (Figure 1D). With the aid of an ionic surfactant, sodium dodecyl benzenesulfonate (SDBS), the dispersion became homogeneous and white-colored after a 3 h ultrasonication process, indicating the efficacy of SDBS for dispersing and debundling BNNT fibrils (Figure 1E). This dispersion was subsequently centrifuged at 5000 rpm at 4 °C for 5 min and the BNNT supernatant was collected for PD coating. After the dopamine self-polymerization reaction, the dispersion was homogeneous and the color turned from white to brown (Figure 1F).

Characterization of PD-Functionalized BNNTs. Low-magnification TEM imaging was performed to assess BNNT

DOI: 10.1021/acs.bioconjchem.5b00257
Bioconjugate Chem. 2015, 26, 2025−2037

dispersion before and after PD functionalization. Specifically, it was observed that SDBS dispersed BNNT suspensions tended to agglomerate into bundles of 4 to 6 μm in diameter (Figure 2A). In contrast, PD coated-BNNTs were well dispersed and when cast onto a surface, formed a percolated network (Figure 2B).

BNNTs were observed to possess well-defined walls, typically ranging in number from 4 to 6. Moreover, the unaltered hexagonal arrangements of B and N atoms were observable in pristine BNNTs (Figure 3A). The presence of an investing PD coating was confirmed by energy-dispersive X-ray spectroscopy (EDS) analysis and high-resolution TEM imaging. TEM analysis also allowed the direct observation of PD functionalization of BNNTs, where it was possible to identify a homogeneous 1.5-nm-thick coating along the nanotube surface (Figure 3B,C). The presence of a superficial PD layer was further confirmed via dynamic light scattering (DLS) and it was noted that following PD functionalization the mean hydrodynamic radius was increased from 228 ± 3 to 257 ± 4 nm (see Supporting Information S1−S3).

EDS analysis of SDBS dispersed BNNTs indicated B and N peaks of similar intensity, and also the presence of SDBS as indicated by the Na and S signals. In contrast, following PD functionalization, Na and S signals were reduced and an increased C signal was obtained (Figure 3D,E).

The presence of PD coating was also confirmed by X-ray photoelectron spectroscopy (XPS) that indicated significant differences in elemental composition between BNNTs and PD-BNNTs (Figure 4). Specifically, the carbon content (as indicated by the C 1s peak) increased from 4.6% for pristine BNNTs to 16.9% for SDBS dispersed BNNTs and to 24.9% for PD-functionalized BNNTs.

To quantify the significant effects of PD functionalization on BNNT dispersion the absorbance profiles of BNNTs, PD, and PD-functionalized BNNTs as a function of the wavelength were quantified (Figure 5). An increase in the absorbance for PD-functionalized BNNTs with respect to SDBS dispersed BNNTs (non-functionalized) was observed. This increase in adsorption was also observed as a function of concentration. Here we assessed absorbance with concentrations ranging from 0 to 0.2 mg/ml. In this manner, it was possible to estimate the final concentration of PD in a PD-functionalized BNNT dispersion following centrifugation. Accordingly, a value around 20 μg/mL was obtained by assessing the absorbance of SDBS dispersed PDs (see Supporting Information S4) and the aid of eq 1. The effects of SDBS coating were further evaluated via UV−Vis analysis (see Supporting Information S5).

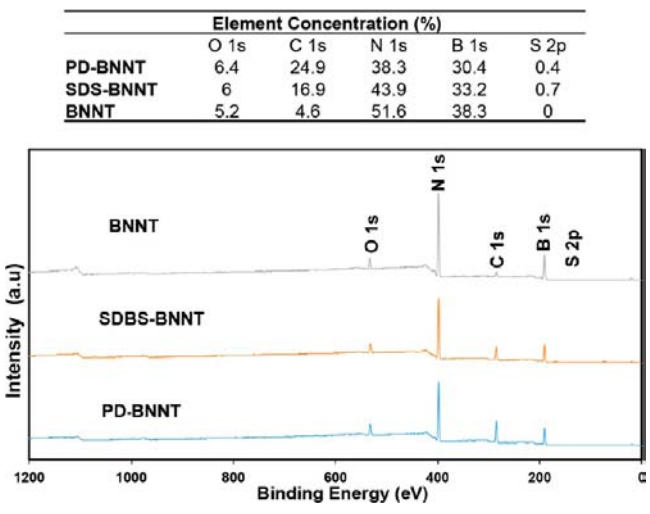

Figure 4. XPS survey spectra and elemental quantification of pristine, SDBS dispersed, and PD-functionalized BNNTs. SDBS dispersion significantly increased the content of carbon (C1 s, 16.9%) and decreased the boron (B 1s, 33.2%) and nitrogen (N 1s, 43.9%) relative to pristine BNNTs. A further significant increase in the carbon content (24.9%) was observed in PD-functionalized BNNTs attributed to the carbon and nitrogen backbone of the PD. Sulfur content (S 2p), originating from SDBS immersion, was present only on SDBS-dispersed (0.7%) and PD-functionalized BNNTs (0.4%).

Cytotoxicity of BNNTs. Osteoblasts were cultured in complete media containing SDBS dispersed and PD-functionalized BNNT's of increasing concentrations. Figures 6 and 7 show representative fluorescent microscopy images of live/dead labeled cells cultured with non-functionalized and functionalized BNNTs respectively, and corresponding concentrations of 1, 10, and 30 μg/mL acquired after 24, 48, and 72 h.

Quantification of cell viability was also performed as a function of fluorescence absorbance. Live/dead assay indicated that after 24, 48, and 72 h of cellular exposure to increasing concentrations (1, 10, and 30 μg/mL) of non-functionalized BNNTs cell viability was significantly reduced relative to that of untreated control situations. However, cell viability was not affected in HOBs cultured with PD-functionalized BNNT relative to control conditions. Indeed, a viability of approximately 90% was maintained in all experimental groups after 72 h (Figure 8A). Similarly, cells exposed to non-functionalized and PD-functionalized BNNTs were observed to undergo differential metabolic activity and proliferation rates. Critically, non-functionalized BNNTs significantly reduced both cellular metabolic activity and cell proliferation relative to control conditions. This effect was reversed in cells cultured with PD-functionalized BNNTs (Figure 8B,C).

In order to assess the cellular internalization of PD-functionalized and non-functionalized BNNTs, biological TEM was performed at day 3 with all BNNT concentrations. It was observed that both non-functionalized (Figure 9) and PD-functionalized (Figure 10) BNNTs became internalized following 72 h of culture and both nano and microscale aggregations of nanotubes and individual nanotubes as single entities were observed to localize to the cell endosomes. Significantly, at concentrations of 30 μg/mL BNNTs become localized to the cell membrane. Evidence of clathrin-dependent endocytosis as an uptake mechanisms (Figures 9D and 10D) was observed for both non-functionalized and PD-functionalized BNNTs. Furthermore, evidence was also noted for the presence of endosomal escape[56] (Figure 10C).

DISCUSSION

In the present work, PD functionalization was employed to improve the dispersion of pressurized vapor/condenser synthesized BNNTs in aqueous solutions and, at the same time, provide functional surface groups as a proof of concept study for future functionalization strategies. To improve the reaction between individual BNNTs and dopamine, BNNTs were first dispersed in Tris-HCl (10 mM, pH = 8.5) with the aid of SDBS, which has been previously employed to improve the dispersion of BNNTs in aqueous solutions.[10,47]

Dispersion was confirmed microscopically with ultra-high-resolution TEM. At low magnification, large BNNT agglomerations were observed in pristine suspensions with few isolated

DOI: 10.1021/acs.bioconjchem.5b00257
Bioconjugate Chem. 2015, 26, 2025−2037

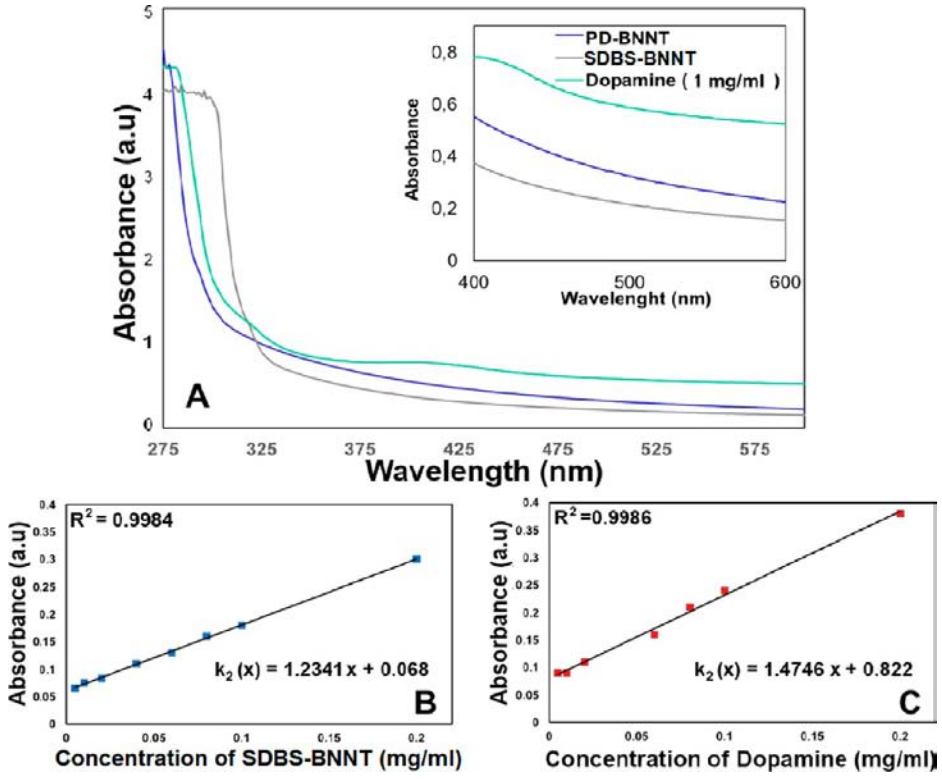

Figure 5. Absorbance spectroscopy of non-functionalized BNNT, PD-functionalized BNNT and PD (0.5 mg/mL) (A), and standard curves showing the extinction coefficients (k_i) for non-functionalized BNNT (B) and Dopamine (C). The correlation of the curve was 99.8% for n = 3 samples.

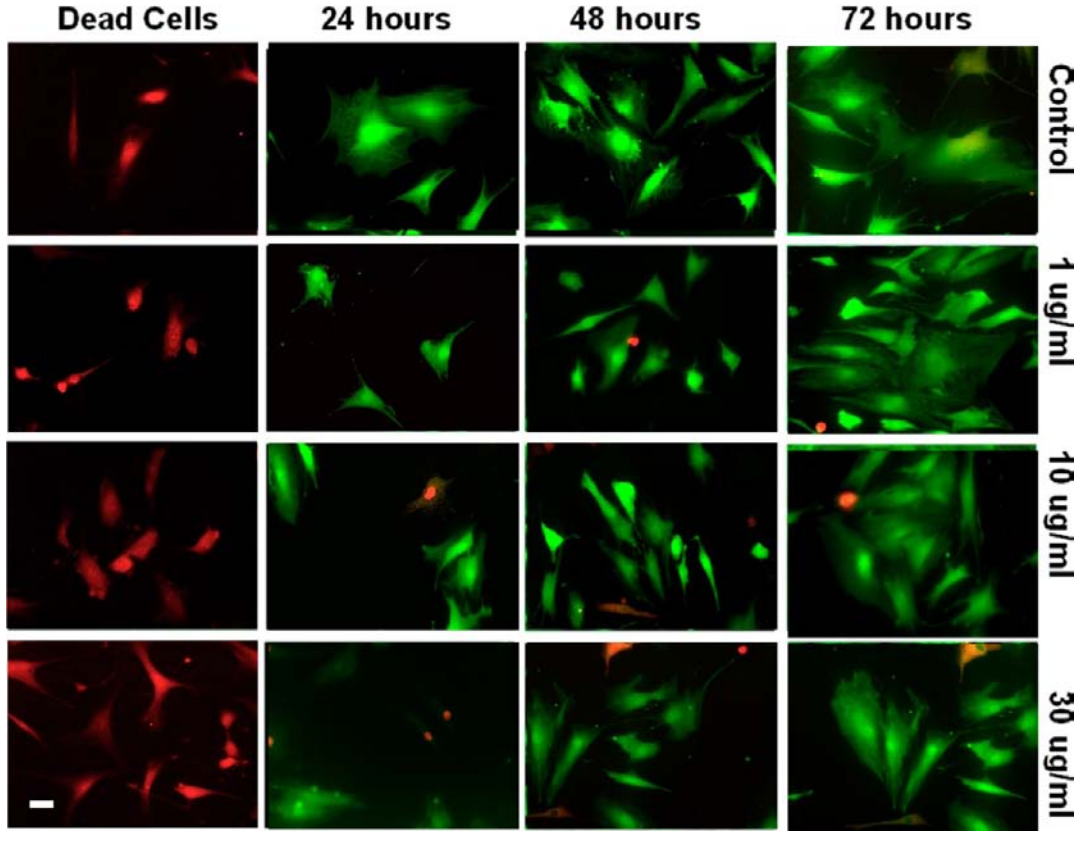

Figure 6. Representative images of Live/Dead Assay for HOBs treated with methanol as a positive control, and 0, 1, 10, and 30 μg/mL of SDBS dispersed BNNTs after 24, 48, and 72 h. Cytotoxicity was noted in cells treated with uncoated SDBS dispersed BNNTs at all concentrations and all time-points. Green—live, Red—dead. Scale bar = 50 μm.

DOI: 10.1021/acs.bioconjchem.5b00257
Bioconjugate Chem. 2015, 26, 2025−2037

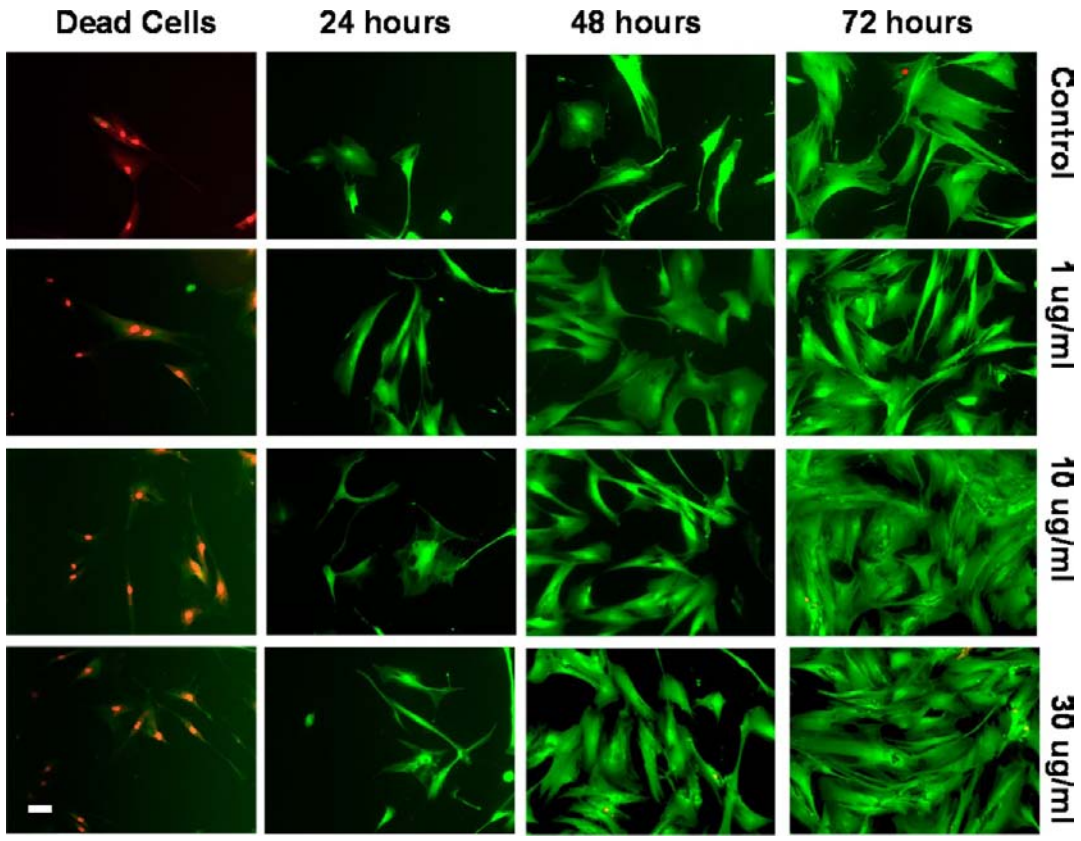

Figure 7. Representative images of Live/Dead Assay for HOBs treated with methanol as a positive control, and 0, 1, 10, and 30 μg/mL of PD-BNNTs after 24, 48, and 72 h. Relative to cells treated with non-functionalized BNNTs, the observable number of nonviable cells was not significant at all concentrations. Green—live, Red—dead. Scale bar = 50 μm.

tubes. Conversely, PD-BNNT suspensions were associated with significantly lower agglomeration and a percolated network of individual nanotubes. Critically, unlike CNTs, the polar B−N bond within BNNTs increases the interconnectivity between individual nanotubes making the dispersion process more difficult.[48]

At high magnification, the number of BNNT walls was measured and its integrity was evaluated. Based on our measurements, the number of walls of BNNTs ranged from 4 to 6. Furthermore, the employed dispersion and functionalization process did not damage the integrity of the wall. Although there is extensive literature concerning different methodologies for dispersion and functionalization of CNTs, many of these produce irreversible changes to the nanotube ultrastructure that can negatively affect the intrinsic properties of the nanotubes.[49,50] The PD layer was clearly discernible with ultra-high-magnification TEM imaging, and a thickness of approximately 1.5 nm was noted. Considering that the backbone of PD is composed predominantly of carbon atoms, the carbon content increase detected by EDS and XPS can be clearly associated with the presence of PD on the surface of BNNTs. Moreover, this PD layer remained stable even after several washing steps, suggesting a strong interaction between the coating and the nanotubes.

Although PD has been widely employed as a functionalization chemistry for various materials in vitro, its mechanism of self-assembly is still under debate and, therefore, the interaction with BNNTs admits several interpretations. So far, the most accepted structure for PD is one composed of dihydroxyindole and indoledione units linked by C−C bonds between their benzene rings. Similarly, the presence of open chain dopamine units within the polymer has been also demonstrated.[57] Herein, it is hypothesized that BNNTs interact with dopamine molecules in solution via strong $\pi-\pi$ stacking forces between aromatic molecules of dopamine and the closed hexagonal structure of BNNTs, as well as via van der Waals interactions between the amino groups of dopamine and the boron atoms of the BNNTs[40,41,51] (Figure 11). Furthermore, the hydrophilic $-$ OH and $-$ NH_2 groups present in PD may facilitate the dispersion of BNNTs in aqueous solutions.

Unlike BNNTs, carbon derived nanomaterials (including, but not limited to, carbon black nanoparticles, carbon quantum dots, single and multiwall nanotubes) have found a wide range of applications, such as drug and gene delivery, scaffolds for tissue engineering, and as a nanoreinforcement material.[40,41] However, in order to make direct comparisons between BNNTs and CNTs a number of parameters should be taken into consideration: length, diameter, concentration, wall number (single or multiwall tubes), and the presence of surface functional groups.

The biological effects of boron nitride nanochemistries have not been extensively assessed, and very few studies have focused on the in vitro compatibility of such.[14,15,42,46] However, a significant number of studies have been conducted on the cytocompatibility of CNTs which indicate that the cytotoxicity, cellular, and immune responses greatly vary, with little consensus as of yet with respect to the mechanisms of action. Similarly, the cytotoxicity of pristine BNNTs has been reported at concentrations as low as 2 μg/mL,[46] while other studies have found pristine BNNTs to be highly biocompatible at

DOI: 10.1021/acs.bioconjchem.5b00257
Bioconjugate Chem. 2015, 26, 2025−2037

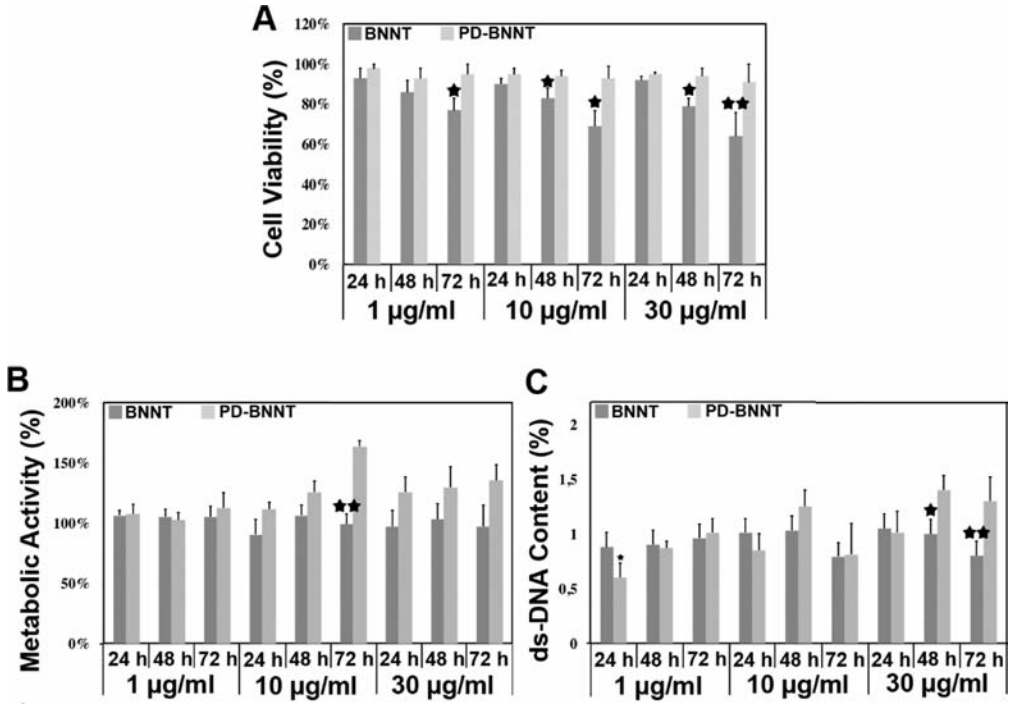

Figure 8. Influence of non-functionalized and PD-functionalized BNNTs on cellular viability, metabolic activity, and proliferation. HOBs were observed following 24, 48, and 72 h of culture with 1, 10, and 30 μg/mL of BNNTs. Cell viability as assed by live/dead assay was significantly reduced in HOBs cultured with non-functionalized BNNTs, yet was unchanged in HOBs cultured with PD-functionalized BNNTs at all time points (A). Metabolic activity as assessed by AlamarBlue analysis indicated a trend of reduced metabolic activity in cells cultured with non-functionalized BNNTs relative to cells cultured with PD-functionalized BNNTs and under control culture conditions (B). Similarly, cellular proliferation as assessed via Pico Green assay indicated significantly reduced cell proliferation in cells cultured in the presence of non-functionalized BNNTs relative to cells cultured with PD-functionalized BNNTs and under control culture conditions at concentrations of 30 μg/mL (C). Results were normalized to control samples for each time point. Results are expressed as mean ± SEM (n = 5), * $P < 0.05$); and ** $P < 0.01$.

concentrations up to 20 μg/mL both in vitro and in vivo.[15,42,43,52,53] These conflicting results may be explained by the different methodologies employed for the manipulation and purification of the nanotubes that result in different surface properties as well as the presence of impurities.[49] Furthermore, the length and the diameter of nanotubes have been shown to determine the mechanisms of cellular interaction and nanotube geometry has been shown to modulate cellular toxicity and particle fate.[59,60]

Critically, it has also been proven that the hydrophobic nature of boron nitride based nanotubes facilitates cellular internalization and negatively affects cell viability. Thus, the need for biofunctionalization seems mandatory.[54] In the case of CNTs, noncovalent functionalization with biopolymers such as PD is proven to be an efficient pathway to solve the problems associated with dispersion, and the use of both synthetic and natural chemistries are gaining more attention for the functionalization of nanoparticle formulations including BNNTs.

In the present study we have investigated the biological effects of non-functionalized and PD-functionalized BNNTs of three different concentrations (1, 10, and 30 μg/mL) and incubation times (24, 48, and 72 h), on HOB viability and activity in vitro. As confirmed by a live/dead assay, significant cytotoxicity was observed in non-functionalized BNNTs at concentrations ≥1 μm/ml, a trend not observed with HOBs exposed to PD-functionalized BNNTs. Furthermore, in order to assess the proliferation rate of HOBs exposed to both non-functionalized and PD-functionalized BNNTs, DNA quantification was conducted via Picogreen analysis, which confirmed that although proliferation decreased as a function of time in HOBs exposed to non-functionalized BNNTs at all concentrations, the proliferation rate was maintained in HOBs exposed to PD-functionalized BNNTs. Similar studies conducted by Ciofani et al. have concluded that 10 μg/mL of poly(L-lysine) (PLL) coated BNNT do not negatively influence viability or function in C2C12 cells after 3 days in culture.[55] Furthermore, tolerable BNNT concentrations were increased to 20 μg/mL when functionalized with polyethylenimine.[53] Interestingly, BNNT functionalization with polymer coatings seems to play a critical role in preventing BNNT cytotoxicity.

A recent study by Horvath et al. concluded that both non-functionalized and acid-treated BNNTs are cytotoxic even at low concentrations.[46] In this study, different cell lines (human embryonic cells and lung alveoli cells) were exposed to pristine and acid-treated BNNTs at different concentrations (0.02, 0.2, 2, and 20 μg/mL). Unfortunately, at present it is not possible to decouple the importance of chemical functionalization in reducing BNNT cytotoxicity from other physical properties such as nanotube dimension and shape, which have been proposed as the principal mediator of BNNT toxicity. In particular, a study of Ciofani et al. on gum Arabic functionalized BNNTs has indicated the importance of the length and aspect ratio of BNNT on cytocompatibility.[58] Here it was noted that the short (1.5 μm) BNNTs employed in their study significantly enhanced cytocompatibility relative to the nanotubes employed by Horvath et al., which possessed lengths of ≥5 μm. This duality of nanotube aspect ratio and surface chemistry in mediating cytotoxicity is also confirmed in the

DOI: 10.1021/acs.bioconjchem.5b00257
Bioconjugate Chem. 2015, 26, 2025−2037

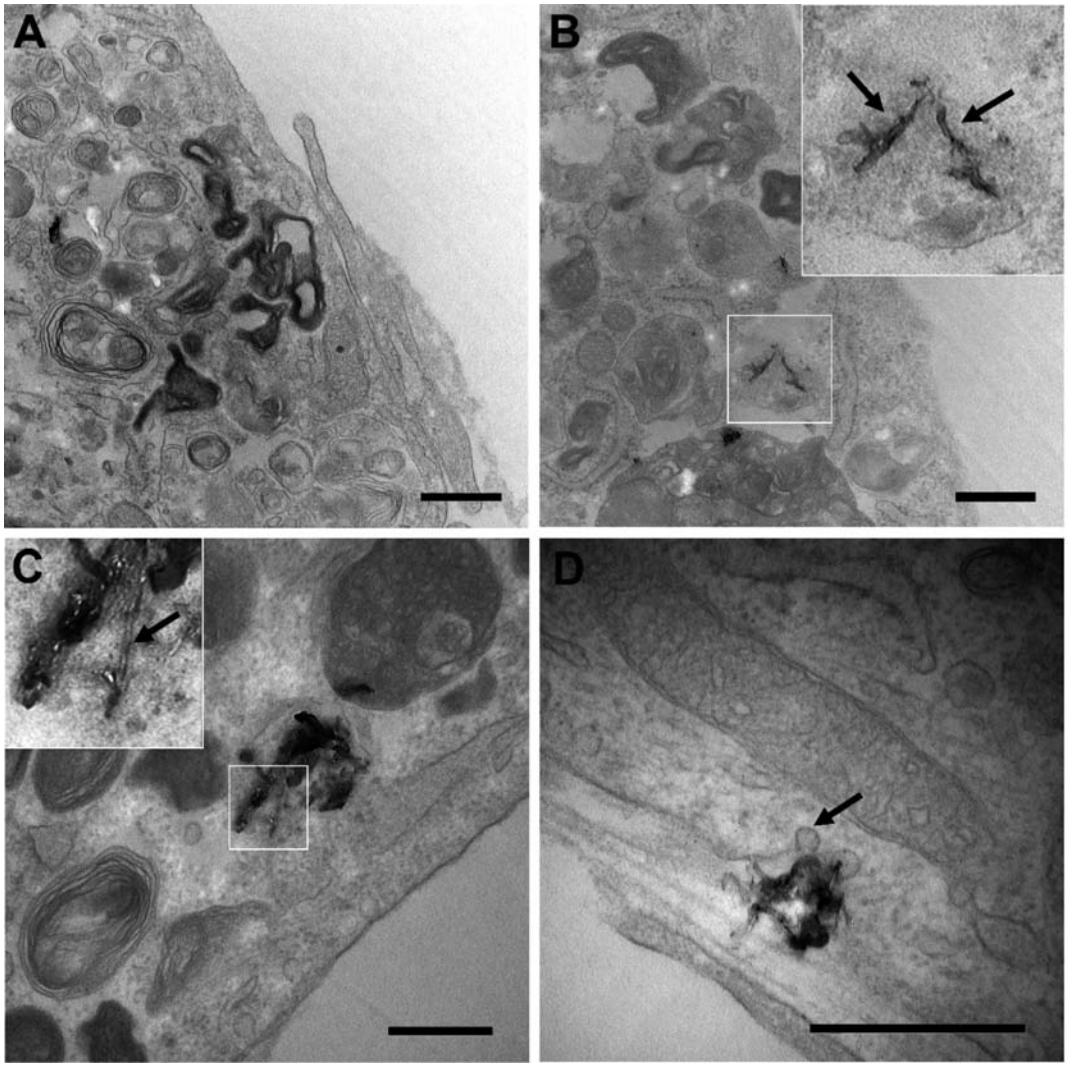

Figure 9. TEM analysis of cellular internalization of non-functionalized BNNTs after 72 h. Low cellular uptake was observed after incubation with, 1, 10, and 30 μg/mL (A, B, and C) of SDBS dispersed BNNTs following 72 h. Internalization of single nanotubes (B) was less frequent then the presence of aggregates of multiple nanotubes (C, D) which were localized within endosomes (arrows). Evidence of clathrin-dependent endocytosis was observed with nanotube aggregates (D). Scale bar = 500 nm.

present study, which utilizes nanotubes with relatively short lengths (1 μm).

Although nanoparticle uptake is reportedly reduced with nanotubes larger than approximately 1 μm,[59] elongated particles including boron nitride nanotubes can be internalized via clatherin-dependent endocytosis as demonstrated in a previous study by Ciofani et al. Here neither C2C12 myoblast viability nor myotube formation was significantly perturbed by BNNT endocytosis following 3 days of culture.[55] Energetically active endocytic processes may also be responsible for BNNT internalization, particularly of aggregated BNNT clusters or of individualized nanotubes which may be captured, fused, or accumulated within lipid-rich vesicular compartments.[61]

In the present study it was observed that internalization of BNNTs into HOBs was via endocytosis; however, the uptake of pristine BNNTs at the same dose was significantly lower. Therefore, it is hypothesized that dopamine coating might allow better dispersion at these concentrations and more efficient cell uptake. Interestingly, it was noted in the present study that BNNTs may be able traverse into the cytoplasmic space. This phenominon has been previously shown with CNTs, which are able to traverse the endosomal membrane by "piercing" and extending into the cell cytoplasm, a process that has been recently described as "endosomal escape".[59] However, a lack of observed toxicity suggests that no significant intracellular interaction between tubes and other intracellular compartments occurred after 72 h.

The experimental data of Jin et al.[33] demonstrated that the highest uptake of nanoparticles occurs with nanotubes 320 ± 30 nm in length and decreases with longer (660 ± 40 nm) and shorter (130 ± 18 nm) nanotubes. Interestingly, it has also been demonstrated previously that agglomerated or relatively long nanotubes become localized to the cell surface to form a protective coating that prevents internalization. In the present study it was noted that cells exposed to 30 μg/mL of PD-functionalized BNNT were associated with aggregates of nanotubes at the extracellular plasma membrane, while BNNT concentrations of 1 μg/mL were well dispersed and significant deposition at the cell surface was not observed.

DOI: 10.1021/acs.bioconjchem.5b00257
Bioconjugate Chem. 2015, 26, 2025−2037

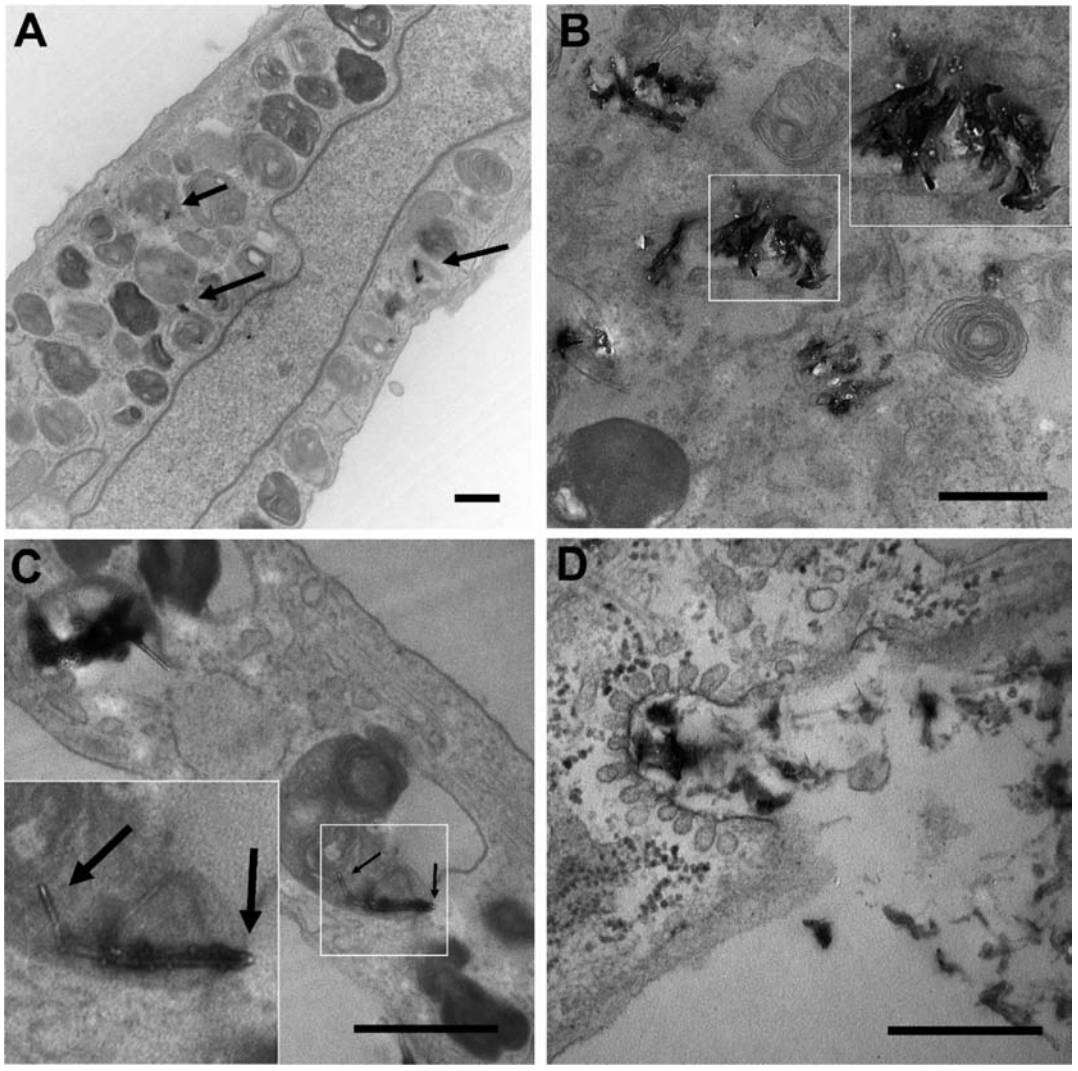

Figure 10. TEM analysis of cellular internalization of PD-functionalized BNNTs after 72 h. Hobs incubated with 1 and 30 μg/mL of BNNTs (A, B) demonstrated significant BNNT internalization at day 3. It was observed that large nanoscale aggregates (B) and individual nanotubes (C) were localized in both endosomes (B) and/or escaping from endosomes into the cytoplasm (C). Evidence of clathrin-dependent endocytosis was again observed with nanotube aggregates (D). Scale bar = 500 nm.

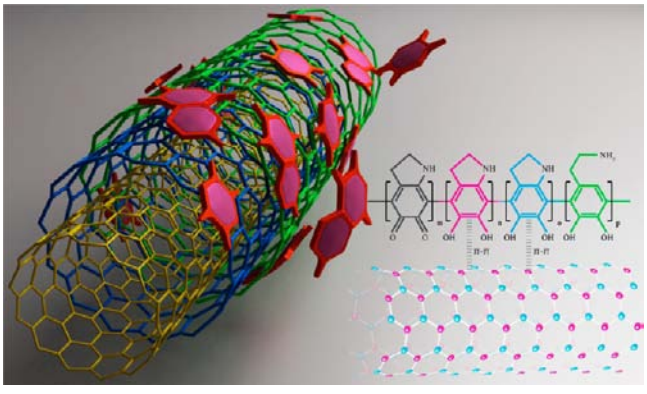

Figure 11. Schematic representation of the most accepted structure of PD and its interaction with BNNT via strong $\pi-\pi$ stacking forces.

CONCLUSIONS

In this study, it has been illustrated that disentanglement by a surfactant assisted ultrasonication process and subsequent functionalization with PD improved the dispersion and stability of BNNTs in aqueous solutions. In addition, in contrast to non-functionalized BNNT dispersions, PD-functionalized BNNTs were not observed to modulate cellular proliferation or metabolic activity. Osteoblasts exhibited no significant cytotoxic effects when cultured with PD-functionalized BNNTs at concentrations from 1 to 30 μg/mL and for up to 72 h of culture. We conclude that PD functionalization can be employed as an effective strategy for the production of well-dispersed and cytocompatible BNNT formulations. These results are in contrast to previous studies, which have reported that cytotoxicity is present in noncoated BNNTs at concentrations greater than 2 μg/mL.[55] Interestingly, we noted that PD-functionalized BNNTs concentrations greater than 10 μg/mL increased the presence of PD-BNNT bundles in solution as a consequence of the ionic strength of media, and became localized to the HOB plasma membrane. Then, it can be hypothesized that highly agglomerated nanotubes may be deposited onto the cell surface acting as a protective layer, which can prevent the endocytosis of isolated nanotubes. PD-functionalized BNNTs at low concentration were internalized by the cell as individual entities. In contrast, low concentrations

DOI: 10.1021/acs.bioconjchem.5b00257
Bioconjugate Chem. 2015, 26, 2025−2037

of pristine BNNT did not allow dispersion and uptake of individual BNNTs.

To evaluate the future biomedical potential of BNNTs and reveal the benefits of these nanoparticles over widely explored CNTs, further research is required, and further investigations into the cellular uptake mechanisms and BNNT interactions with cellular compartments should be at the forefront of this research. We conclude that dopamine coating can be employed as an effective strategy for the production of well-dispersed and cytocompatible BNNT formulations.

MATERIALS AND METHODS

Materials. BNNTs were purchased from BNNT, LLC, USA) and synthesized using a high temperature/pressure (HTP) method, also called the pressurized vapor/condenser method (PVC). The purity is reportedly approximately 50% by mass containing residual impurities as microdroplets of elemental boron.[11] Dopamine hydrochloride was purchased from Sigma-Aldrich (H8502, MW: 189.64 g/mol) and was utilized for BNNT coating. SDBS (28995, Sigma-Aldrich) acts as an ionic surfactant for achieving a good dispersion prior to PD coating. 300 mesh lacey carbon film grids were purchased from Agar Scientific. Normal Human Osteoblasts (NHOst), and Clonetics Osteoblast Growth Media were purchased from Lonza. Quant-IT Picogreen dsDNA Assay kit (P11496), alamarBlue Cell Viability reagent (DAL110) and Live/Dead Cytotoxicity Kit for mammalian cells (3224) were purchased from Life Technologies (Thermo Fisher Scientific).

Methods. *Coating of BNNTs with PD.* The schematic representation of the BNNT functionalization process with PD is illustrated in Figure 1. BNNTs were originally obtained as sponges composed of dense fibrils. Prior to PD coating, BNNTs were dispersed with the aid of the ionic surfactant SDBS. 400 μg of BNNTs were mixed with 10 mL of Tris-HCl (pH 8.5) solution containing 500 μg of SDBS. This mixture was then sonicated for 3 h (pulse 10 s ON, 2 s OFF) with an output power of 17 W. Subsequently, the homogenized dispersion was centrifuged at 5000 rpm (2516 *g*) for 5 min at 4 °C to remove BNNT aggregates and impurities and the supernatant was collected. The concentration of BNNTs in the supernatant was 180 μg/mL, determined via spectrophotometric (Varioskan Flash Multimode Reader, UV−Vis) analysis after obtaining the extinction coefficient of BNNTs for determining their concentration (calibration curve with known concentrations of BNNTs is shown in Supporting Information S4 and S5). Dopamine hydrochloride (1 mg/mL) was then added to the dispersion and stirred for 18 h at RT. During this process, the color of the dispersion turned from white to brown due to the oxidation and self-polymerization of dopamine. Finally, BNNTs were collected by centrifugation at 13 000 rpm (17 005 *g*) and washed twice with distilled water to remove unreacted dopamine. In this manner, pellets of BNNTs were obtained for further physicochemical characterization and cell culture studies (Figure 1). The final PD-BNNT dispersion in DI water was stable for up to 2 months without any precipitation confirmed by DLS measurements. Finally, pellets of SDBS and PD-BNNT were directly dispersed by ultrasonication (15 min) in protein free media for further incorporation into cell culture.

Characterization of BNNTs. *High-Magnification Transmission Electron Microscopy (TEM).* Samples for high-magnification nonbiological TEM were prepared by depositing one drop of a diluted dispersion of BNNTs onto a lacey carbon grid and drying overnight. Samples were exanimated with a JEOL JEM-2100 F TEM operated at 200 kV using a Field Emission Electron Gun equipped with a Gatan Ultrascan digital camera and an EDAX Genesis XM 4 energy dispersive X-ray (EDS) analyzer. The probe size chosen for EDS analysis was set to 1.5 nm to obtain high-resolution and sufficient signal from the area of interest. TEM was performed in order to both characterize the morphology of BNNT dispersion by measuring the diameter of BNNT aggregations and to evaluate the uniformity of the PD coating.

X-ray Photoelectron Spectroscopy. XPS analysis was performed in a Kratos AXIS Ultra spectrometer using monochromatic Al Kα radiation of energy 1486.6 eV. Low-resolution spectra of B 1s, C 1s, N 1s, O 1s, and S 2p were taken at fixed pass energy of 20 eV. Surface charge was efficiently neutralized by flooding the sample surface with low energy electrons. Binding energies were determined using C 1s peak at 284.8 eV as charge reference. For construction and fitting of synthetic peaks of low-resolution spectra, a mixed Gaussian-Lorenzian function with a Shirley type background subtraction was used.

Dynamic Light Scattering (DLS). DLS was utilized to determine the size distribution of BNNTs before and after PD coating with a Malvern Nano-ZS90. Each measurement represents the average value of 10−15 measurements with 20 s integration time for each measurement. All the experiments were carried out at 25 °C in a ZEN0112 disposable cuvette.

UV−visible Spectroscopy. A Varioskan Flash plate reader for luminescent assays was used to assess BNNT concentrations in aqueous media. The spectrophometric values obtained on well-dispersed nanotubes permitted the evaluation of the extinction coefficient. In addition, after PD coating, the measurement of residual PD in solution and onto the nanotube surfaces was realized based on a simultaneous analysis of two-component mixture by UV−Vis. Although it was expected that PD coating can affect the light-absorbing properties of the BNNT, it was possible to quantify the amount of PD within a given range. If the absorption of the light by the two-component additive was considered, then we can determine the amount of PD present by the following equation:

$$A = k_1C_1 + k_2C_2 \quad (1)$$

where k is the extinction coefficient and C the concentration of each solute. By choosing two different wavelengths, two equations with two unknowns were generated. Note that the two chosen wavelengths can be the same used for obtaining the extinction coefficient (Beer's Law plot). The chosen wavelengths were 400 and 600 nm (Supporting Information S4).

Cell Culture and Cytocompatibility Assays. Normal human osteoblasts (NHOst, Lonza, USA) were cultured in Dulbecco's Modified Eagle Media (DMEM; Sigma), supplemented with 10% fetal bovine serum (FBS; Sigma), 100 μg/mL of penicillin, and 100 μg/mL of streptomycin in an atmosphere of 5% CO_2 at 37 °C and media was changed every 2 days. All assays were conducted on cells from passage 5 to 6. A cell suspension was obtained by addition of 5% trypsin with EDTA (Lonza, USA). After flushing and centrifugation, the cells were resuspended in DMEM supplemented medium and the number of viable cells was estimated with Trypan Blue exclusion and a hemocytometer. Next, viable cells were seeded as below for cell viability analysis. Cells were maintained in culture for up to 3 days and cell viability/cytotoxicity tests were conducted at days 1, 2, and 3.

DOI: 10.1021/acs.bioconjchem.5b00257
Bioconjugate Chem. 2015, 26, 2025−2037

Live/Dead (Cell Viability) Quantification. Viable cells were seeded at a density of 5000 per well in 96-well ($n = 5$) plates for quantitative analysis and in 4-well glass bottom chamber slide for fluorescent microscopy. Osteoblasts were cultured overnight and BNNTs were added to the well plates/slides after 12 h and incubated for a further 24, 48, or 72 h. Untreated live and dead cells were used as controls for quantitative analysis. To induce HOB death, cells were incubated for 5 min with 70% methanol. Live/Dead Assay (Life Technologies) was used to visualize viable and necrotic cells. After coincubation, samples were washed with PBS and stained with calcein and ethidium bromide from the kit as recommended by manufacturer. The cells were incubated with the stock solution for 30 min protected from light. The well plates were immediately analyzed with a Varioskan Flash plate reader. Samples were subsequently imaged on an Olympus IX81 inverted fluorescent microscopy with 20× and 100× objectives.

Double-Stranded-DNA (ds-DNA) Quantification. Quant-iT Pico Green ds-DNA Assay Kit was employed to assess cell proliferation. Cells were seeded in a 96-well plate to a density of 5000 cells per well, 24 h prior to the addition of BNNTs. Different concentrations (1, 10, or 30 mg/mL) of BNNTs were added in complete medium containing 10% FCS and cells were cultured as described previously. After 24, 48, or 72 h in culture the cells were processed via a PicoGreen assay according to the manufacturers protocol. Briefly, cell lysis to release the DNA was performed by a freeze−thaw process. Subsequently, 25 μL of the lysis sample was mixed with 25 μL of TE buffer and 50 μL of a working solution of Picrogreen dye in 96-well plate. After incubation for 5 min at RT the fluorescence intensity was measured (exc. 435 nm; emi. 535 nm) using a Varioskan Flash plate reader.

Metabolic Activity Quantification. AlamarBlue was used to examine cell metabolic activity. Briefly, HOBs were seeded into 24-well plates at a density of 20,000 cells per well. The cells were left to attach overnight in humidified atmosphere, 37 °C, 5% CO_2. After 12 h, BNNTs of concentrations ranging 1, 10, and 30 mg/mL were added to the cells as described previously. Fluorescence intensity analysis was performed on Varioskan Flash plate reader. Untreated cells were used as controls.

Biological TEM Sample Preparation and Image Acquisition. Following 3 days of culture with functionalized and nonfunctionalized BNNTs at 1, 10, and 30 μg/mL samples were subjected to three washes using prewarmed 0.1 M Na-Cacodylate buffer (37 °C) and fixed for 30 min using 4% paraformaldehyde, 2% Glutaraldehyde in 0.1 M Na-Cacodylate buffer. Following fixation, cells were washed 3 times using 0.1 M Na-Cacodylate buffer and postfixed using 1% osmium tetroxide in 0.1 M Na-Cacodylate buffer for 20 min. Cells were then dehydrated through a graded series of ethanol (30%, 50%, 70%, 90%, and 100% each 2× 10 min). For the final ethanol step, 1 mL was added to each T25 flask and cells were removed from the flask using a cell scrapper and then transferred to 1.5 mL Eppendorf tubes and pelleted at 4000 rpm for 5 min. Cell pellets were incubated in propylene oxide (intermediate solvent) for 30 min and then infiltrated and embedded with TAAB low viscosity resin according to standard protocol. For orientation purposes semithin sections (1 μm) were cut and stained by toluidine blue. Subsequently, ultrathin sections (90 nm) were cut and left unstained. Ultrathin sections were examined with a Hitachi H-7000 electron microscope fitted with a 1K Hammamatsu Digital Camera. Images were captured using AMTV542 Image Capture Engine software.

Stastical Analysis. All data were analyzed using Minitab 17. Analysis of variance (ANOVA) with Tukey's comparisons posthoc tests were performed after confirming the following assumptions: (a) the distribution from which each of the samples was derived was normal; and (b) the variances of the population of the samples were equal to one another. Statistical significance was accepted at $p < 0.05$.

■ ASSOCIATED CONTENT

Supporting Information

The Supporting Information is available free of charge on the ACS Publications website at DOI: 10.1021/acs.bioconjchem.5b00257.

BNNT dispersion with SDBS and subsequent functionalization with PD was assessed via dynamic light scattering and UV−Vis analysis. Dynamic light scattering spectra confirmed a significant reduction in the hydrodynamic radius of BNNTs extracted from the supernatant as a function of centrifugation speed (S1 and S2), and a further reduction in hydrodynamic radius following PD functionalization (S3). Quantification of PD in solution (S4) and the dispersing power of SDBS on BNNTs (S5) were subsequently assessed through UV−Vis spectroscopy. Here a significant reduction in absorbance was observed with PD functionalization over wavelengths ranging 300−1000 nm. (PDF)

■ AUTHOR INFORMATION

Corresponding Author

*E-mail: manus.biggs@nuigalway.ie.

Notes

The authors declare no competing financial interest.

■ ACKNOWLEDGMENTS

M.J.B. would like to acknowledge Science Foundation Ireland, Starting Investigators Research Program, under the grant agreement number 11/SIRG/B2135, and the Science Foundation Ireland Centre for Research in Medical Devices (CÚRAM) (Grant agreement number 13/RC/2073). The authors would like to thank Maciek Doczyk (http://doczykdesign.com) for his support in the preparation of the figures in this manuscript. We would like to thank Dr. Kerry Thompson, Dr. Peter Owens, and Mr. Pierce Lalor of the Centre of Microscopy & Imaging at the National University of Ireland, Galway (www.imaging.nuigalway.ie), cofunded by the Irish Government and the European Union under Ireland's EU Structural Funds Program. A.L. would like to acknowledge Basque Government (Department of Education, Language Policy and Culture).

■ REFERENCES

(1) Lahiri, D., Rouzaud, F., Richard, T., Keshri, A. K., Bakshi, S. R., Kos, L., and Agarwal, A. (2010) Boron nitride nanotube reinforced polylactide-polycaprolactone copolymer composite: mechanical properties and cytocompatibility with osteoblasts and macrophages in vitro. *Acta Biomater. 6*, 3524−33.

(2) Karagkiozaki, V., Karagiannidis, P. G., Kalfagiannis, N., Kavatzikidou, P., Patsalas, P., Georgiou, D., and Logothetidis, S. (2012) Novel nanostructured biomaterials: implications for coronary stent thrombosis. *Int. J. Nanomed. 7*, 6063−76.

(3) Zheng, F., Zhou, G., Hao, S., and Duan, W. (2005) Structural characterizations and electronic properties of boron nitride nanotube crystalline bundles. *J. Chem. Phys. 123*, 124716.

DOI: 10.1021/acs.bioconjchem.5b00257
Bioconjugate Chem. 2015, 26, 2025−2037

(4) Nigues, A., Siria, A., Vincent, P., Poncharal, P., and Bocquet, L. (2014) Ultrahigh interlayer friction in multiwalled boron nitride nanotubes. *Nat. Mater. 13*, 688−93.
(5) Polizu, S., Savadogo, O., Poulin, P., and Yahia, L. (2006) Applications of carbon nanotubes-based biomaterials in biomedical nanotechnology. *J. Nanosci. Nanotechnol. 6*, 1883−904.
(6) Popov, A. M., Lozovik, Y. E., Fiorito, S., and Yahia, L. (2007) Biocompatibility and applications of carbon nanotubes in medical nanorobots. *International journal of nanomedicine 2*, 361−72.
(7) Ciofani, G., Danti, S., Genchi, G. G., D'Alessandro, D., Pellequer, J. L., Odorico, M., Mattoli, V., and Giorgi, M. (2012) Pilot in vivo toxicological investigation of boron nitride nanotubes. *Int. J. Nanomed. 7*, 19−24.
(8) Zhi, C., Bando, Y., Shen, G., Tang, C., and Golberg, D. (2007) Boron nitride nanotubes: nanoparticles functionalization and junction fabrication. *J. Nanosci. Nanotechnol. 7*, 530−4.
(9) Yamaguchi, M., Pakdel, A., Zhi, C., Bando, Y., Tang, D. M., Faerstein, K., Shtansky, D., and Golberg, D. (2013) Utilization of multiwalled boron nitride nanotubes for the reinforcement of lightweight aluminum ribbons. *Nanoscale Res. Lett. 8*, 3.
(10) Zheng, M., Chen, X., Park, C., Fay, C. C., Pugno, N. M., and Ke, C. (2013) Nanomechanical cutting of boron nitride nanotubes by atomic force microscopy. *Nanotechnology 24*, 505719.
(11) Kalay, S., Yilmaz, Z., Sen, O., Emanet, M., Kazanc, E., and Culha, M. (2015) Synthesis of boron nitride nanotubes and their applications. *Beilstein J. Nanotechnol. 6*, 84−102.
(12) Danti, S., Ciofani, G., Pertici, G., Moscato, S., D'Alessandro, D., Ciabatti, E., Chiellini, F., D'Acunto, M., Mattoli, V., and Berrettini, S. (2015) Boron nitride nanotube-functionalised myoblast/microfibre constructs: a nanotech-assisted tissue-engineered platform for muscle stimulation. *Journal of tissue engineering and regenerative medicine 9*, 847−851.
(13) Ciofani, G., Del Turco, S., Genchi, G. G., D'Alessandro, D., Basta, G., and Mattoli, V. (2012) Transferrin-conjugated boron nitride nanotubes: protein grafting, characterization, and interaction with human endothelial cells. *Int. J. Pharm. 436*, 444−53.
(14) Ferreira, T. H., Hollanda, L. M., Lancellotti, M., and de Sousa, E. M. (2015) Boron nitride nanotubes chemically functionalized with glycol chitosan for gene transfection in eukaryotic cell lines. *J. Biomed. Mater. Res., Part A 103*, 2176−85.
(15) Ferreira, T. H., Soares, D. C., Moreira, L. M., da Silva, P. R., dos Santos, R. G., and de Sousa, E. M. (2013) Boron nitride nanotubes coated with organic hydrophilic agents: stability and cytocompatibility studies. *Mater. Sci. Eng., C 33*, 4616−23.
(16) Zhi, C., Bando, Y., Tang, C., and Golberg, D. (2005) Immobilization of proteins on boron nitride nanotubes. *J. Am. Chem. Soc. 127*, 17144−5.
(17) Ciofani, G., Raffa, V., Menciassi, A., and Dario, P. (2008) Preparation of boron nitride nanotubes aqueous dispersions for biological applications. *J. Nanosci. Nanotechnol. 8*, 6223−31.
(18) Yu, A., Bekyarova, E., Itkis, M. E., Fakhrutdinov, D., Webster, R., and Haddon, R. C. (2006) Application of centrifugation to the large-scale purification of electric arc-produced single-walled carbon nanotubes. *J. Am. Chem. Soc. 128*, 9902−8.
(19) Anson-Casaos, A., Gonzalez, M., Gonzalez-Dominguez, J. M., and Martinez, M. T. (2011) Influence of air oxidation on the surfactant-assisted purification of single-walled carbon nanotubes. *Langmuir 27*, 7192−8.
(20) Hu, H., Yu, A., Kim, E., Zhao, B., Itkis, M. E., Bekyarova, E., and Haddon, R. C. (2005) Influence of the zeta potential on the dispersability and purification of single-walled carbon nanotubes. *J. Phys. Chem. B 109*, 11520−4.
(21) Li, J., Chajara, K., Lindgren, J., and Grennberg, H. (2007) Rapid acid-mediated purification of single-walled carbon nanotubes with homogenization of bulk properties. *J. Nanosci. Nanotechnol. 7*, 1525−9.
(22) Barattin, R., and Voyer, N. (2008) Chemical modifications of AFM tips for the study of molecular recognition events. *Chem. Commun.*, 1513−32.
(23) Fujigaya, T., Yamamoto, Y., Kano, A., Maruyama, A., and Nakashima, N. (2011) Enhanced cell uptake via non-covalent decollation of a single-walled carbon nanotube-DNA hybrid with polyethylene glycol-grafted poly(l-lysine) labeled with an Alexa-dye and its efficient uptake in a cancer cell. *Nanoscale 3*, 4352−8.
(24) Qiao, R., and Ke, P. C. (2006) Lipid-carbon nanotube self-assembly in aqueous solution. *J. Am. Chem. Soc. 128*, 13656−7.
(25) Doss, J., Olubi, O., Sannigrahi, B., Williams, M. D., Gadi, D., Baird, B., and Khan, I. (2012) Procedure for fabricating biofunctional nanofibers. *J. Visualized Exp.*, DOI: 10.3791/4135.
(26) Zhang, G., Jia, X., Liu, Z., Hu, J., Ma, Z., and Zhou, F. (2013) Protein resistance and pH-responsive controlled release from the modification of single-walled carbon nanotubes with a double polymer layer. *Macromol. Biosci. 13*, 1259−66.
(27) Sesis, A., Hodnett, M., Memoli, G., Wain, A. J., Jurewicz, I., Dalton, A. B., Carey, J. D., and Hinds, G. (2013) Influence of acoustic cavitation on the controlled ultrasonic dispersion of carbon nanotubes. *J. Phys. Chem. B 117*, 15141−50.
(28) Sauer, U. G., Aumann, A., Ma-Hock, L., Landsiedel, R., and Wohlleben, W. (2015) Influence of dispersive agent on nanomaterial agglomeration and implications for biological effects in vivo or in vitro. *Toxicol. In Vitro 29*, 182−6.
(29) Chang, X., Henderson, W. M., and Bouchard, D. C. (2015) Multiwalled Carbon Nanotubes Dispersion Methods Affect Their Aggregation, Deposition, and Biomarker Response. *Environ. Sci. Technol. 49*, 6645.
(30) Strano, M. S., Moore, V. C., Miller, M. K., Allen, M. J., Haroz, E. H., Kittrell, C., Hauge, R. H., and Smalley, R. E. (2003) The role of surfactant adsorption during ultrasonication in the dispersion of single-walled carbon nanotubes. *J. Nanosci. Nanotechnol. 3*, 81−6.
(31) Shen, K., Curran, S., Xu, H., Rogelj, S., Jiang, Y., Dewald, J., and Pietrass, T. (2005) Single-walled carbon nanotube purification, pelletization, and surfactant-assisted dispersion: a combined TEM and resonant micro-raman spectroscopy study. *J. Phys. Chem. B 109*, 4455−63.
(32) Ruan, B., and Jacobi, A. M. (2012) Ultrasonication effects on thermal and rheological properties of carbon nanotube suspensions. *Nanoscale Res. Lett. 7*, 127.
(33) Zaib, Q., Khan, I. A., Yoon, Y., Flora, J. R., Park, Y. G., and Saleh, N. B. (2012) Ultrasonication study for suspending single-walled carbon nanotubes in water. *J. Nanosci. Nanotechnol. 12*, 3909−17.
(34) Lee, Y. B., Shin, Y. M., Lee, J. H., Jun, I., Kang, J. K., Park, J. C., and Shin, H. (2012) Polydopamine-mediated immobilization of multiple bioactive molecules for the development of functional vascular graft materials. *Biomaterials 33*, 8343−52.
(35) Lee, J. S., Lee, K., Moon, S. H., Chung, H. M., Lee, J. H., Um, S. H., Kim, D. I., and Cho, S. W. (2014) Mussel-inspired cell-adhesion peptide modification for enhanced endothelialization of decellularized blood vessels. *Macromol. Biosci. 14*, 1181−9.
(36) Lee, H., Dellatore, S. M., Miller, W. M., and Messersmith, P. B. (2007) Mussel-inspired surface chemistry for multifunctional coatings. *Science 318*, 426−30.
(37) Lynge, M. E., van der Westen, R., Postma, A., and Stadler, B. (2011) Polydopamine–a nature-inspired polymer coating for biomedical science. *Nanoscale 3*, 4916−28.
(38) Ryu, J., Ku, S. H., Lee, H., and Park, C. B. (2010) Mussel-Inspired Polydopamine Coating as a Universal Route to Hydroxyapatite Crystallization. *Adv. Funct. Mater. 20*, 2132−2139.
(39) Yang, L., Phua, S. L., Toh, C. L., Zhang, L., Ling, H., Chang, M., Zhou, D., Dong, Y., and Lu, X. (2013) Polydopamine-coated graphene as multifunctional nanofillers in polyurethane. *RSC Adv. 3*, 6377−6385.
(40) Thakur, V. K., Yan, J., Lin, M.-F., Zhi, C., Golberg, D., Bando, Y., Sim, R., and Lee, P. S. (2012) Novel polymer nanocomposites from bioinspired green aqueous functionalization of BNNTs. *Polym. Chem. 3*, 962−969.
(41) Wu, H., and Kessler, M. R. (2015) Multifunctional Cyanate Ester Nanocomposites Reinforced by Hexagonal Boron Nitride after

DOI: 10.1021/acs.bioconjchem.5b00257
Bioconjugate Chem. 2015, 26, 2025−2037

Noncovalent Biomimetic Functionalization. *ACS Appl. Mater. Interfaces 7*, 5915−5926.
(42) Danti, S., Ciofani, G., Moscato, S., D'Alessandro, D., Ciabatti, E., Nesti, C., Brescia, R., Bertoni, G., Pietrabissa, A., Lisanti, et al. (2013) Boron nitride nanotubes and primary human osteoblasts: in vitro compatibility and biological interactions under low frequency ultrasound stimulation. *Nanotechnology 24*, 465102.
(43) Salvetti, A., Rossi, L., Iacopetti, P., Li, X., Nitti, S., Pellegrino, T., Mattoli, V., Golberg, D., and Ciofani, G. (2015) In vivo biocompatibility of boron nitride nanotubes: Effects on stem cell biology and tissue regeneration in planarians. *Nanomedicine 10*, 1−12.
(44) Michalski, P. J., Sai, N., and Mele, E. J. (2005) Continuum Theory for Nanotube Piezoelectricity. *Phys. Rev. Lett. 95*, 116803.
(45) Fernandez-Yague, M. A., Abbah, S. A., McNamara, L., Zeugolis, D. I., Pandit, A., and Biggs, M. J. (2015) Biomimetic approaches in bone tissue engineering: Integrating biological and physicomechanical strategies. *Adv. Drug Delivery Rev. 84*, 1−29.
(46) Horvath, L., Magrez, A., Golberg, D., Zhi, C., Bando, Y., Smajda, R., Horvath, E., Forro, L., and Schwaller, B. (2011) In vitro investigation of the cellular toxicity of boron nitride nanotubes. *ACS Nano 5*, 3800−10.
(47) Zheng, M., Ke, C., Bae, I.-T., Park, C., Smith, M. W., and Jordan, K. (2012) Radial elasticity of multi-walled boron nitride nanotubes. *Nanotechnology 23*, 095703.
(48) Zhi, C., Bando, Y., Tang, C., Xie, R., Sekiguchi, T., and Golberg, D. (2005) Perfectly dissolved boron nitride nanotubes due to polymer wrapping. *J. Am. Chem. Soc. 127*, 15996−7.
(49) Zhang, Y., Wang, B., Meng, X., Sun, G., and Gao, C. (2011) Influences of acid-treated multiwalled carbon nanotubes on fibroblasts: proliferation, adhesion, migration, and wound healing. *Ann. Biomed. Eng. 39*, 414−26.
(50) Vittorio, O., Raffa, V., and Cuschieri, A. (2009) Influence of purity and surface oxidation on cytotoxicity of multiwalled carbon nanotubes with human neuroblastoma cells. *Nanomedicine 5*, 424−31.
(51) Shen, H., Guo, J., Wang, H., Zhao, N., and Xu, J. (2015) Bioinspired Modification of h-BN for High Thermal Conductive Composite Films with Aligned Structure. *ACS Appl. Mater. Interfaces 7*, 5701−5708.
(52) Del Turco, S., Ciofani, G., Cappello, V., Gemmi, M., Cervelli, T., Saponaro, C., Nitti, S., Mazzolai, B., Basta, G., and Mattoli, V. (2013) Cytocompatibility evaluation of glycol-chitosan coated boron nitride nanotubes in human endothelial cells. *Colloids Surf., B 111*, 142−9.
(53) Ciofani, G., Raffa, V., Menciassi, A., and Cuschieri, A. (2008) Cytocompatibility, interactions, and uptake of polyethyleneimine-coated boron nitride nanotubes by living cells: confirmation of their potential for biomedical applications. *Biotechnol. Bioeng. 101*, 850−8.
(54) Gao, Z., Zhi, C., Bando, Y., Golberg, D., Komiyama, M., and Serizawa, T. (2012) Efficient disentanglement of boron nitride nanotubes using water-soluble polysaccharides for protein immobilization. *RSC Adv. 2*, 6200−6208.
(55) Ciofani, G., Ricotti, L., Danti, S., Moscato, S., Nesti, C., D'Alessandro, D., Dinucci, D., Chiellini, F., Pietrabissa, A., Petrini, M., et al. (2010) Investigation of interactions between poly-L-lysine-coated boron nitride nanotubes and C2C12 cells: up-take, cytocompatibility, and differentiation. *International journal of nanomedicine 5*, 285−98.
(56) Al-Jamal, K. T., et al. (2011) Cellular uptake mechanisms of functionalised multi-walled carbon nanotubes by 3D electron tomography imaging. *Nanoscale 3*, 2627−2635.
(57) Liebscher, J., et al. (2013) Structure of polydopamine: a never-ending story? *Langmuir 29*, 10539−10548.
(58) Ciofani, G., et al. (2014) Cytocompatibility evaluation of gum Arabic-coated ultra-pure boron nitride nanotubes on human cells. *Nanomedicine (London, U. K.) 9*, 773−788.
(59) Al-Jamal, K. T., et al. (2011) Cellular uptake mechanisms of functionalised multi-walled carbon nanotubes by 3D electron tomography imaging. *Nanoscale 3*, 2627−2635.
(60) Jin, H., et al. (2009) Size-dependent cellular uptake and expulsion of single-walled carbon nanotubes: single particle tracking and a generic uptake model for nanoparticles. *ACS Nano 3*, 149−158.
(61) Mu, Q., et al. (2009) Endosomal leakage and nuclear translocation of multiwalled carbon nanotubes: developing a model for cell uptake. *Nano Lett. 9*, 4370−4375.

DOI: 10.1021/acs.bioconjchem.5b00257
Bioconjugate Chem. 2015, 26, 2025−2037